IMPEDANCE MATRIX COMPRESSION WITH THE USE OF WAVELET EXPANSIONS

Z. Baharav and Y. Leviatan
Department of Electrical Engineering
Technion-Israel Institute of Technology
Haifa 32000, Israel

KEY TERMS

Wavelet, electromagnetic scattering, numerical method

ABSTRACT

Wavelet expansions have been used recently in numerical solutions of integral equations encountered in various electromagnetic scattering problems. In these solutions one utilizes the power of the wavelet basis functions to localize the problem impedance matrix. Thus, after the impedance matrix has been computed, it can be rendered sparse via a thresholding procedure, and the resultant matrix equation can be solved in more quickly without any significant loss in accuracy. In this article we propose a novel approach, where instead of thresholding the impedance matrix in a conventional manner, it is compressed to a reduced-size form. This is effected by first singling out a small number of basis functions, which are expected to accurately represent the unknown, and keeping only the matrix elements needed for finding the coefficients of these basis functions. A method to carry out this matrix compression automatically is described. Numerical examples are given for the case of TM scattering by perfectly conducting cylinders of triangular and square cross sections. The advantages of the proposed approach are shown.

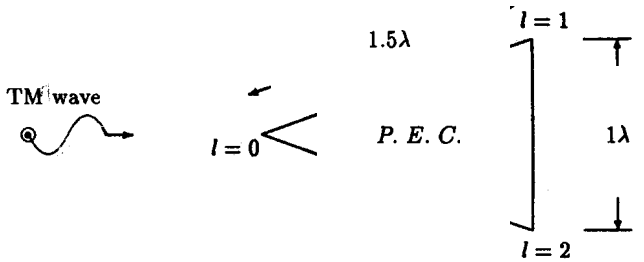

Figure 1 Scattering problem geometry for the first example

where $[\mathcal{Z}]$ is the impedance matrix, **A** is the vector of unknown current coefficients, and **B** is the excitation vector.

3. REDUCING THE SIZE OF THE IMPEDANCE MATRIX

Once the matrix equation for the problem is obtained, we proceed toward reducing its size, while minimizing the loss in accuracy, using the following matrix compression procedure. Suppose that only a small number of the wavelet functions in the series expansion (2) is required to accurately represent J_z, and that we know how to single these few wavelet functions out. In other word, assume that there exists a subset $\{W_{i(k)}\}_{k=1}^{M}$, M being much smaller than N, which can represent J_z to an acceptable accuracy. Then we have

$$J_z' = \sum_{k}^{M} A'_{i(k)} W_{i(k)}, \tag{4}$$

where the primes affixed to J_z' and $A'_{i(k)}$ indicate that these quantities, although close, are not necessarily identical to their unprimed counterparts. To determine the coefficients $\{A'_{i(k)}\}_{k=1}^{M}$, we construct a new matrix $[\mathcal{Z}']$ comprising only the columns $\{i(k)\}_{k=1}^{M}$ of $[\mathcal{Z}]$. The matrix $[\mathcal{Z}']$ is substantially smaller in size compared to $[\mathcal{Z}]$, and hence the computation of the coefficients $\{A'_{i(k)}\}$ is relatively faster.

It is worth mentioning again that the resulting coefficients $\{A'_{i(k)}\}_{k=1}^{M}$ may differ from their unprimed counterparts. This is due to the fact that although the wavelet basis functions are orthogonal, the field functions these source functions produce are not. Another point worthy of consideration is the possibility of proportionally reducing the number of equations as well. Choosing the equations that can be omitted without having a dramatic effect on the value of the coefficient should generally be done with caution, because one must also ensure that the boundary conditions are still satisfied. In the matrices considered here, the number of rows is taken to be twice the number of columns.

So far we have assumed that we know which are the dominant terms in the wavelet expansion for the unknown current. But one can justifiably argue that in general it is difficult to determine which of the terms will be more dominant. This is where the underlying physics of the problem emerge. As we know from physical optics, the value of the excitation on the surface can be indicative as to the current. Therefore, the idea is to represent the excitation vector by the wavelet basis functions, determine the indices of the dominant coefficients of this decomposition, and choose the subset of wavelet functions accordingly. Of course, this method is only approximate; moreover, it does not take into account the shadow regions of the body. However, as will be shown in the next section, owing to the apparent correlation between the current and the excitation vectors when they each are expressed in a series of wavelet basis functions, this method is quite useful.

4. NUMERICAL EXAMPLES

To show the advantages of the new approach, we first consider the problem of scattering by a perfectly conducting cylinder of triangular cross section. The incident wave is a TM_Z (transverse magnetic) plane wave, and the configuration, with related parameters, is shown in Figure 1. The quantity we wish to determine is the current induced on the cylinder surface. The perimeter of the triangle is divided into 64 pulses. The wavelet basis functions used are the Haar basis functions. The longest basis functions are composed of $2^6 = 64$ pulses. Thus, the basis function of minimum spatial variation constitutes a constant current along the perimeter. A larger number (128) of testing points is specified on the perimeter.

The three cases, namely, applying a thresholding operation on the original impedance matrix obtained by using pulses as basis functions, applying a similar thresholding operation but on the localized matrix obtained by using wavelet basis functions, and compressing the localized matrix obtained by using wavelet basis functions, are compared with each other in Figure 2. This figure shows a plot of the boundary condition error as a function of the compression level. The boundary condition error is defined as the average square error on the scatterer surface normalized to the average square incident field on the scatterer surface. The compression level conveys a measure of the reduction in the number of impedance matrix elements. Naturally, it has to be defined in a slightly different manner for each of the two approaches. In the conventional thresholding approach, the compression is equivalent to the achieved sparseness level defined as the ratio between the number of zero elements in the resultant matrix and the total number of matrix elements. In the approach proposed here it is defined as the ratio

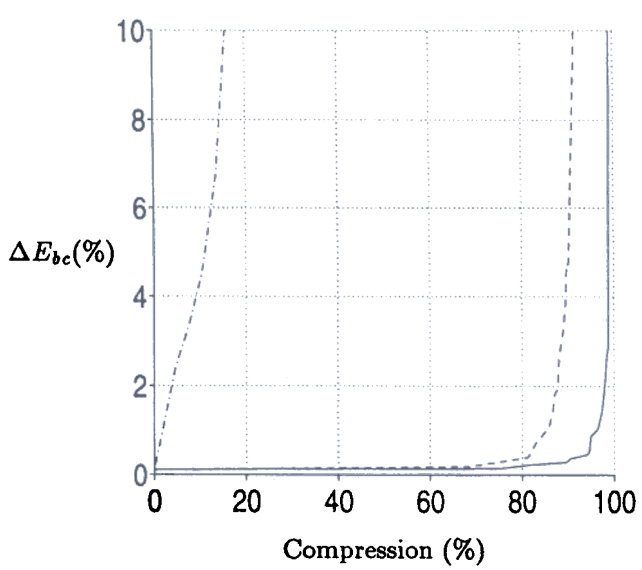

Figure 2 Boundary condition error versus impedance matrix compression level. Cases shown are for thresholding the original impedance matrix as is (dash-dotted line); thresholding the localized matrix, obtained by using Haar wavelet basis functions (dashed line); and compressing the localized matrix by choosing dominant terms (solid line)

between the number of elements omitted the impedance matrix is cast into the compressed form, and the number of elements in the original matrix. If one examines Figure 2, it can be noted that, when no compression of the matrix is taking place, neither thresholding nor reduction of size, the three cases produce *exactly* the same result. However, when compression is applied, the difference in performance is evident, and it is clearly seen that the new method is preferable.

The solution obtained for the current on the scatterer without compression of the impedance matrix, is shown in Figure 3. Additional insight into the new method is given in Figure 4, where the sums of the first few dominant contributors in the series expansion of the current J_z are shown for

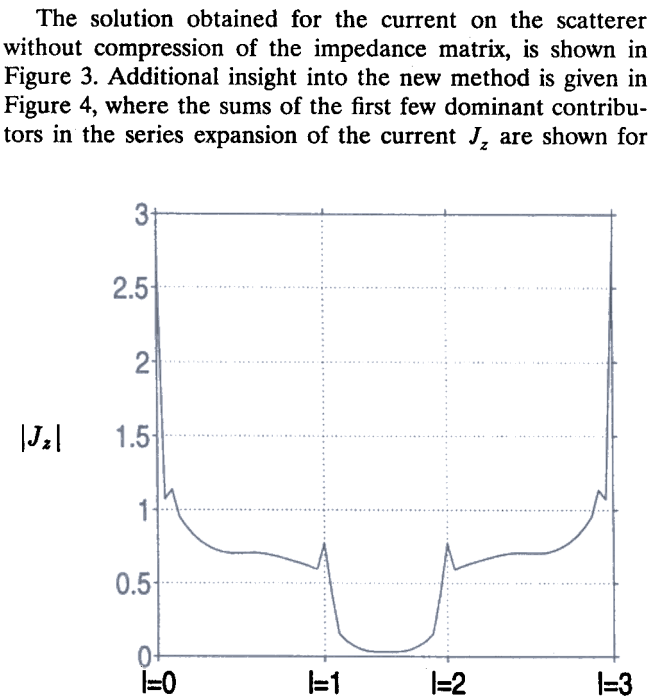

Figure 3 Surface current magnitude (normalized to incident magnetic field) versus the perimetric length variable l

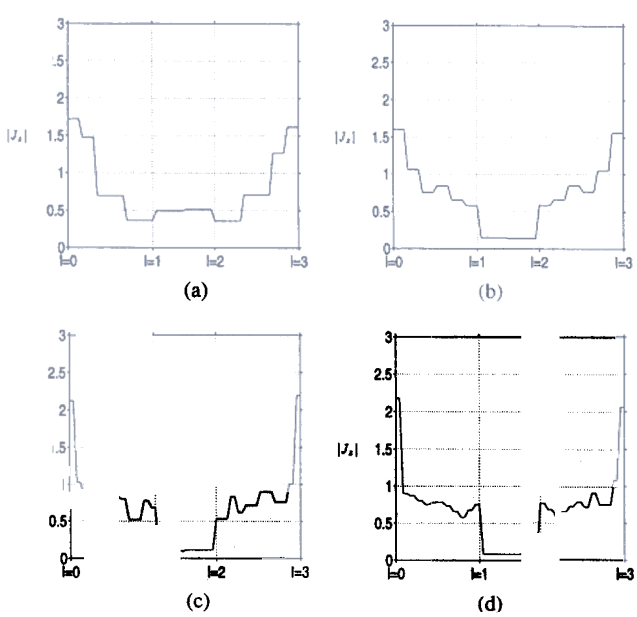

Figure 4 Magnitude of J_z along the triangular perimeter obtained by taking partial sums from the 64-term series expansion. Cases considered are for (a) 7 dominant terms (compression level of 98.7%), (b) 13 dominant terms (compression level of 95%), (c) 19 dominant terms (compression level of 90%), and (d) 24 dominant terms (compression level of 81%)

the case in which the basis functions are wavelets. In these figures one can literally see how the fine details of the signal are gradually added as more elements in the partial sum are considered. The objective here is merely to exhibit the evolution of the result for the current distribution as more terms are added. Of course, if we keep adding terms, settling for lower compression levels, the result will approach that depicted in Figure 3. Further understanding can be gained by examining the result for the current shown in Figure 5. This result has been obtained upon applying conventional thresholding, which yielded sparsification of exactly the same compression level as that of the case of Figure 4(d). A comparison between Figures 5 and 4(d) gives another clear evidence of the superiority of the proposed approach.

The correlation between the representations of the current and the excitation is examined for pulse and wavelet expansions in Figure 6. Figure 6(a) shows that there is very little correlation between the coefficients of the current and the excitation when they are expanded in a series of pulse functions. On the other hand, from Figure 6(b) one can see that there is a close resemblance between these coefficients when the expansion is in a series of wavelet functions. One more word is in order about the way the information

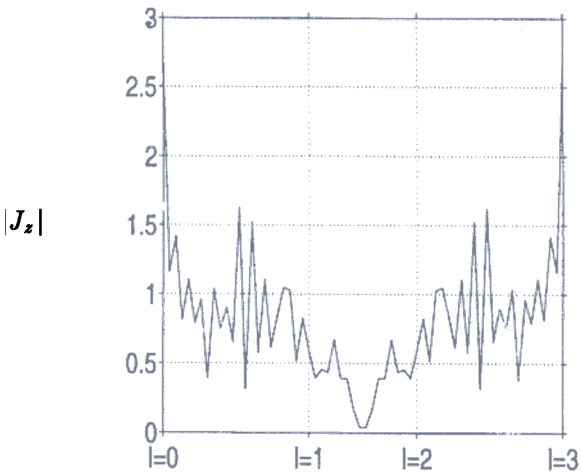

Figure 5 Magnitude of J_z along the triangular perimeter obtained upon sparsifying the wavelet-based impedance matrix to a compression level of 81% by a thresholding operation

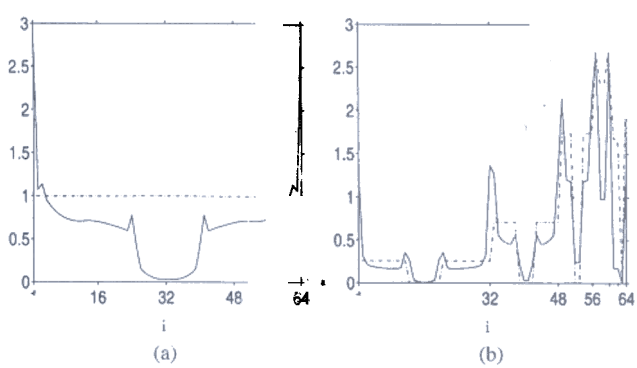

Figure 6 Magnitude of coefficients in the series expansions of the current (solid line) and of the excitation (dashed line) versus serial index i. Cases considered are for (a) standard expansion in a series of pulse basis functions and (b) expansion in a series of Haar wavelet basis functions

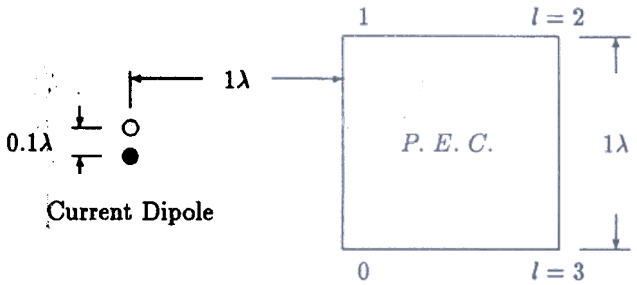

Figure 7 Scattering problem geometry for the second example

is displayed in the figure. The elements in Figure 6(b) are ordered in accordance with the conventional wavelet-coefficient scheme; namely, the first 32 coefficients are the coefficients of the shortest wavelets, those of length $2^1 = 2$. The next 16 coefficients, numbered 33–48, correspond to wavelets of length $2^2 = 4$, and so on. This configuration allows us to identify different regions of the scatterer with the associated coefficients. Thus, for example, the shadow region, which ranges between $l = 1$ and $l = 2$, is clearly identified.

It is important to stress again that regions that are in the shadow of the scatterer are not reflected in the excitation vector. This is because the excitation vector is related to the incident field calculated with the scatterer absent, and hence the interception due to the scatterer is not manifested in the excitation vector. In the discussed example, the excitation vector is simply constant over the shadow region, which implies that all the wavelet functions, which are not constant in this region, will have zero coefficients in the excitation vector series expansion.

The second example deals with a different geometry and a different excitation. The analysis is now applied to the problem of scattering by a perfectly conducting cylinder of square cross section. The excitation is due to two adjacent current

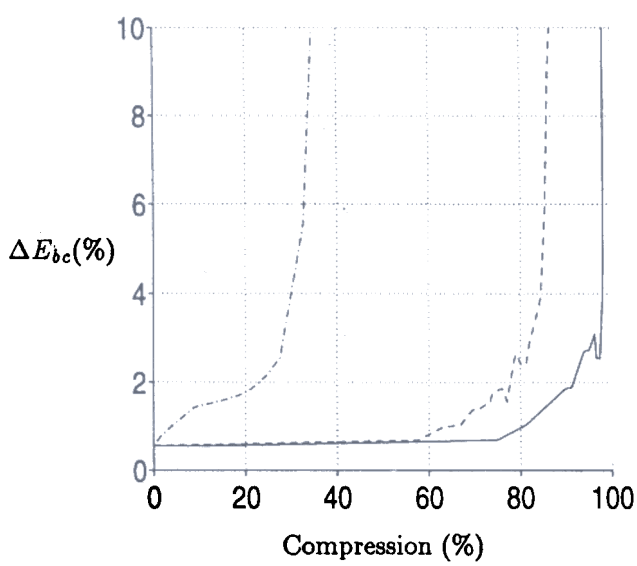

Figure 8 Boundary condition error versus impedance matrix compression level. Cases shown are for thresholding the original impedance matrix as is (dash-dotted line); thresholding the localized matrix, obtained by using Haar wavelet basis functions (dashed line); and compressing the localized matrix by choosing dominant terms (solid line)

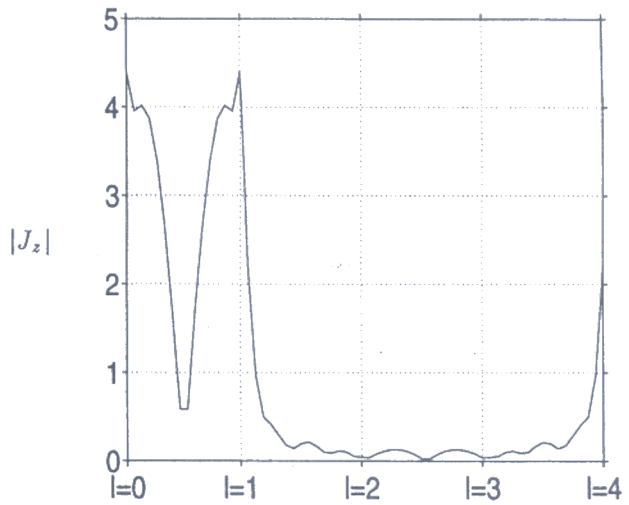

Figure 9 Surface current magnitude (normalized to incident magnetic field) versus the perimetric length variable l

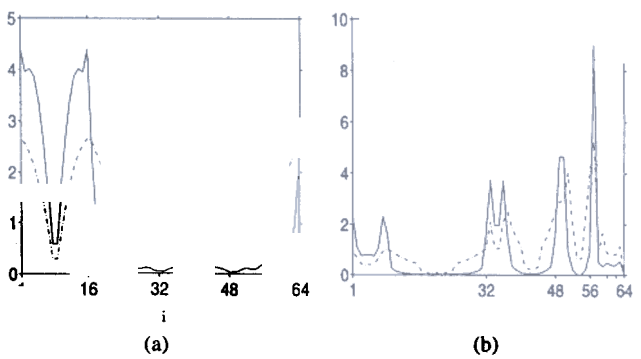

Figure 10 Magnitude of coefficients in the series expansions of the current (solid line) and of the excitation (dashed line) versus serial index i. Cases considered are for (a) expansion in a series of pulse basis functions and (b) expansion in a series of Haar wavelet basis functions

filaments of equal magnitude and opposite polarity. The configuration, with related parameters, is shown in Figure 7. The quantity we wish to determine is the current on the surface of the cylinder. For the numerical solution, the square is also divided into 64 pulses, and a larger number (128) of testing points is selected. The three distinct ways of compressing the impedance-matrix are compared with each other in Figure 8, in a manner similar to that discussed before. Again, the differences in performance are clearly seen. Figure 9 shows the resultant current on the scatterer, when no compression is performed. Figure 10 compares between the pulse and wavelet representations of the current and the excitation. The correlation is again much better for the wavelet representation.

5. SUMMARY AND CONCLUSIONS

In this article we have described a new method for the incorporation of the wavelet basis functions into existing numerical solvers. The new method deals with a new way of reducing the size of the impedance matrix. Thus, instead of using a thresholding procedure, a selective reduction is performed based on the physical understanding of the problem.

This compression procedure was
olding procedure in two examples.

REFERENCES

1. B. Z. Steinberg and Y. Leviatan, "On the Use of Wavelet Expansions in the Method of Moments," *IEEE Trans. Antennas Propagat.*, Vol. AP-41, May 1993, pp. 610–619.
2. H. Kim and H. Ling, "On the Application of Fast Wavelet Transform to the Integral-Equation Solution of Electromagnetic Scattering Problems," *Microwave Opt. Technol. Lett.*, Vol. 6, March 1993, pp. 168–173.
3. R. L. Wagner, G. P. Otto, and W. C. Chew, "Fast Waveguide Mode Computation Using Wavelet-Like Basis Functions," *IEEE Microwave Guided Wave Lett.*, Vol. MGW-3, July 1993, pp. 208–210.
4. K. F. Sabetfakhri and L. P. B. Katehi, "Analysis of Integrated Millimeter-Wave and Submillimeter-Wave Waveguides Using Orthonormal Wavelet Expansions," *IEEE Trans. Microwave Theory Tech.*, Vol. MTT-42, Dec. 1994, pp. 2412–2422.
5. B. Z. Steinberg and Y. Leviatan, "Periodic Wavelet Expansions for Analysis of Scattering from Metallic Cylinders," *Microwave Opt. Technol. Lett.*, Vol. 7, April 1994, pp. 266–268.
6. N. Morita, N. Kumagai, and J. R. Mautz, *Integral Equation Methods for Electromagnetics*. Artech House, Boston, 1990.

Received 3-5-96

Microwave and Optical Technology Letters, 12/ 268–272

CCC 0895-2477/96

MULTIMODE EQUIVALENT NETWORK REPRESENTATION FOR PLANAR JUNCTIONS INVOLVING ELLIPTICAL WAVEGUIDES

B. Gimeno* and M. Guglielmi
European Space Research and Technology Centre (ESTEC)
Postbus 299
2200 AG Noordwijk
The Netherlands

KEY TERMS

Elliptical waveguides, microwave filters, microwave networks

ABSTRACT

Elliptical waveguides and irises are important for application in wideband filters and advanced dual-mode filters. In this Letter we present a general formulation for the multimode equivalent network representation of planar waveguide junctions involving elliptical waveguides. The modes of the elliptical waveguide are obtained by transforming the Helmholtz equation in elliptical coordinates into an equivalent linear matrix eigenvalue equation so that the use of Mathieu functions is avoided. Finally, numerical and experimental results for a number of junctions are presented, and good agreement is found. © 1996 John Wiley & Sons, Inc.

I. INTRODUCTION

Elliptical waveguides have already been analyzed in the technical literature, and there are, in fact, several papers discussing the evaluation of their modes [1–6]. However, no contribution is actually available (to the authors' knowledge) for the study of planar waveguide junctions involving elliptical waveguides.

In this work we develop a multimode equivalent network representation for junctions involving elliptical, rectangular, and circular waveguides based on the multimode admittance coupling matrix [10]. Furthermore, we also develop an efficient approach to obtain the modal spectrum in elliptical waveguide regions, in order to avoid the direct use of the Mathieu functions. Finally, several application examples are discussed, showing very good agreement between measured and simulated results.

II. MULTIMODE EQUIVALENT NETWORK REPRESENTATION OF JUNCTIONS INVOLVING ELLIPTICAL WAVEGUIDES

The problem investigated in this article is the junction between a larger arbitrary waveguide (Region 1) and a smaller elliptical waveguide (Region 2), as shown in Figure 1. For the sake of space, only circular, rectangular, and elliptical waveguides are discussed. The objective is to develop a multimode equivalent network representation (of the type shown in Figure 1) that can be used to study complex waveguide devices composed of cascaded junctions. Following [10], we first define two reference planes denoted as T and T', as shown in Figure 1, and we then write directly the expressions for the admittance coupling matrix elements, obtaining

$$Y_{m,n}^{(1,1)} = -jY_n^{(1)} \cot(\beta_n^{(1)} L)\delta_{m,n},$$

$$Y_n' = Y_n^{(1)} \quad jY_n^{(1)} \operatorname{cosec}(\beta_n^{(1)} L)\langle \mathbf{h}_n^{(1)}, \mathbf{h}_m^{(2)} \rangle \qquad (2)$$

$$Y_{m,n}^{(2,2)} = -j \sum_{k=1} Y_k^{(1)} \cot(\beta_k^{(1)} L)\langle \mathbf{h}_k^{(1)}, \mathbf{h}_m^{(2)} \rangle^{(2)} \langle \mathbf{h}_k^{(1)}, \mathbf{h}_n^{(2)} \rangle$$

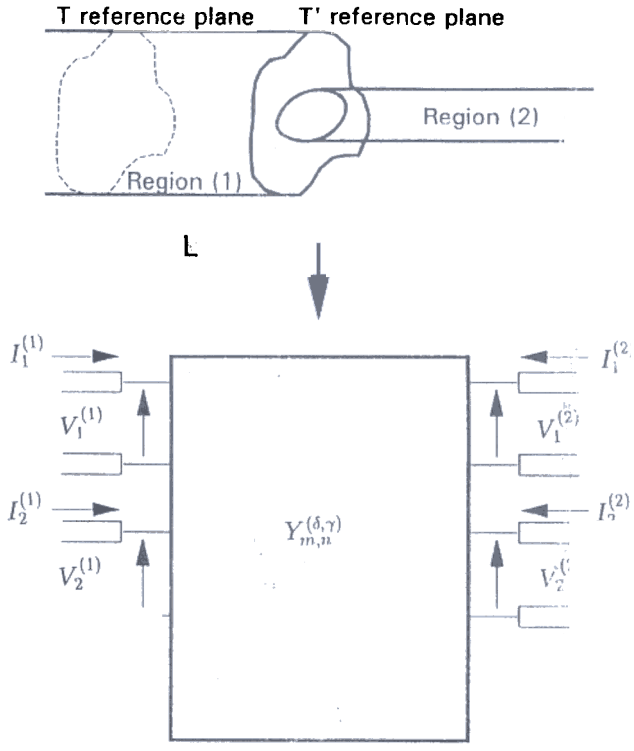

Figure 1 Discontinuity between an arbitrary cross section (Region 1) and elliptical (Region 2) waveguides analyzed in this work together with its multimode equivalent network representation

* Permanent address: Departamento de Fisica Aplicada, Universidad de Valencia, Dr. Moliner, 50, 46100 Burjasot (Valencia), Spain